THE JOURNAL OF BIOLOGICAL CHEMISTRY VOL. 287, NO. 12, pp. 8904–8911, March 16, 2012

Mechanisms of Host Receptor Adaptation by Severe Acute Respiratory Syndrome Coronavirus*[S]

Received for publication, November 21, 2011, and in revised form, January 26, 2012 Published, JBC Papers in Press, January 30, 2012, DOI 10.1074/jbc.M111.325803

Kailang Wu[‡1], **Guiqing Peng**[‡1], **Matthew Wilken**[‡1], **Robert J. Geraghty**[§], **and Fang Li**[‡2]

From the [‡]*Department of Pharmacology and* [§]*Center for Drug Design, University of Minnesota Medical School, Minneapolis, Minnesota 55455*

Background: The severe acute respiratory syndrome (SARS) virus has undergone mutations in its receptor-binding domain.
Results: We used biochemical, functional, and crystallographic methods to investigate these mutations.
Conclusion: These mutations were viral adaptations to either the human or palm civet receptor.
Significance: This research elucidates detailed mechanisms of host receptor adaptation by the SARS virus and can help predict and monitor future evolution of the SARS virus in animals.

The severe acute respiratory syndrome coronavirus (SARS-CoV) from palm civets has twice evolved the capacity to infect humans by gaining binding affinity for human receptor angiotensin-converting enzyme 2 (ACE2). Numerous mutations have been identified in the receptor-binding domain (RBD) of different SARS-CoV strains isolated from humans or civets. Why these mutations were naturally selected or how SARS-CoV evolved to adapt to different host receptors has been poorly understood, presenting evolutionary and epidemic conundrums. In this study, we investigated the impact of these mutations on receptor recognition, an important determinant of SARS-CoV infection and pathogenesis. Using a combination of biochemical, functional, and crystallographic approaches, we elucidated the molecular and structural mechanisms of each of these naturally selected RBD mutations. These mutations either strengthen favorable interactions or reduce unfavorable interactions with two virus-binding hot spots on ACE2, and by doing so, they enhance viral interactions with either human (hACE2) or civet (cACE2) ACE2. Therefore, these mutations were viral adaptations to either hACE2 or cACE2. To corroborate the above analysis, we designed and characterized two optimized RBDs. The human-optimized RBD contains all of the hACE2-adapted residues (Phe-442, Phe-472, Asn-479, Asp-480, and Thr-487) and possesses exceptionally high affinity for hACE2 but relative low affinity for cACE2. The civet-optimized RBD contains all of the cACE2-adapted residues (Tyr-442, Pro-472, Arg-479, Gly-480, and Thr-487) and possesses exceptionally high affinity for cACE2 and also substantial affinity for hACE2. These results not only illustrate the detailed mechanisms of host receptor adaptation by SARS-CoV but also provide a molecular and structural basis for tracking future SARS-CoV evolution in animals.

Many viruses, particularly RNA viruses, can rapidly adapt to changes in their hosts due to the high mutation rates of these viruses. Such viral adaptation to hosts imposes huge threats to human health because it allows viruses to emerge from animals to infect humans. Understanding viral adaptation to hosts would allow humans to track viral evolution that may lead to viral epidemics, but current knowledge of the mechanisms of viral adaptation to hosts is limited. This study investigates the mechanisms of host receptor adaptation by the severe acute respiratory syndrome coronavirus (SARS-CoV),[3] the agent of the SARS epidemic, and provides a molecular and structural basis for monitoring future SARS-CoV evolution in animals.

SARS broke out as a worldwide epidemic in 2002–2003, causing >8000 human infections with a 10% fatality rate (1–4). SARS briefly recurred in 2003–2004, causing sporadic human infections with mild symptoms and no human-to-human transmission (5–7). Since the SARS epidemic, various SARS-CoV strains have been isolated from humans and palm civets (see Fig. 1*A*). The prototypic human strain, hTor02, was isolated during the 2002–2003 SARS epidemic (8). A strain common to humans and civets, hcGd03, was isolated during the 2003–2004 sporadic SARS infections (6, 7). Strain cSz02 was isolated from civets in animal markets in southern China during the SARS outbreak (5). Strain cHb05 was isolated from wild civets in central China several years after the SARS outbreak (9). In addition, human strain hHae08 was isolated after adaptation of SARS-CoV to human airway epithelial cells *in vitro* (10). Because of the extremely high genetic similarity (~99%) between human and civet SARS-CoV, it is believed that civets

* This work was supported, in whole or in part, by National Institutes of Health Grant R01 AI089728 (to F. L.). This work was also supported by a University of Minnesota Academic Health Center faculty research development grant (to F. L.) and by a Minnesota Partnership for Biotechnology and Medical Genomics grant (to the University of Minnesota).
[S] This article contains supplemental Fig. S1.
The atomic coordinates and structure factors (codes 3SCI, 3SCJ, 3SCK, and 3SCL) have been deposited in the Protein Data Bank, Research Collaboratory for Structural Bioinformatics, Rutgers University, New Brunswick, NJ (http://www.rcsb.org/).
[1] These authors contributed equally to this work.
[2] To whom correspondence should be addressed: Dept. of Pharmacology, University of Minnesota Medical School, 6-121 Jackson Hall, 321 Church St. SE, Minneapolis, MN 55455. Tel.: 612-625-6149; Fax: 612-625-8408; E-mail: lifang@umn.edu.

[3] The abbreviations used are: SARS-CoV, severe acute respiratory syndrome coronavirus; SLCV, SARS-like coronavirus; ACE2, angiotensin-converting enzyme 2; hACE2, human ACE2; cACE2, civet ACE2; RBD, receptor-binding domain; RBM, receptor-binding motif.

played a direct role in transmitting SARS-CoV to humans and were responsible for both of the human SARS infections (5, 11, 12). Although SARS-like coronaviruses (SLCVs) have been isolated from bats, the genetic difference between SLCVs and human or civet SARS-CoV is much greater than that between human and civet SARS-CoV (13, 14). Moreover, SLCVs cannot infect human or civet cells, and SARS-CoV cannot infect bats (15). Because of the direct role of civets in the past SARS epidemic, this study focused on SARS-CoV strains isolated from humans and civets.

Receptor recognition is the first step in viral infection of host cells and one of the most important determinants of viral infectivity and pathogenesis. Although many other host and viral factors can also affect the efficiency of infection and replication of a virus in a specific host, these factors come into play only after a virus has bound to a receptor on the cell membrane. A trimeric spike protein on the SARS-CoV envelope mediates viral entry into host cells. It first binds to its host receptor, angiotensin-converting enzyme 2 (ACE2) (16), and subsequently fuses host and viral membranes (17–19). A defined receptor-binding domain (RBD) on the SARS-CoV spike protein is sufficient for high-affinity binding to ACE2 (20–22). The RBD/ACE2 binding affinity has been established as a key element of SARS-CoV pathogenesis and cross-species infections (10, 11, 23–25). The crystal structure of hTor02 RBD complexed with human ACE2 (hACE2) showed that the RBD contains two subdomains, a core structure and a receptor-binding motif (RBM) that directly binds ACE2 (see Fig. 1*B*) (26). Using hTor02 RBD as a reference, numerous naturally selected mutations have been identified in the RBDs of different SARS-CoV strains isolated from humans or civets. The majority of these mutations fall in the RBM region (see Fig. 1, *A* and *B*). To date, research has focused on two of these mutations, N479K and T487S (7, 11, 24, 27, 28). Biochemical studies showed that both mutations N479K and T487S significantly decrease the RBD/hACE2 binding affinity (24, 28). Structural studies revealed that mutation N479K introduces an energetically unfavorable positive charge at the RBD/hACE2 interface, whereas mutation T487S removes an energetically favorable hydrophobic interaction with hACE2 Lys-353 (see Fig. 1*C*) (26, 27). The molecular and structural mechanisms of all of the other RBM mutations are poorly understood. It is not known why any of these RBM mutations were naturally selected or which RBM mutations were viral adaptations to which host.

Here, we investigated the role of each of the RBM mutations in viral interactions with hACE2 and civet ACE2 (cACE2) using a combination of biochemical, functional and crystallographic methods. Our results show that all of the above RBM mutations were viral adaptations to two "virus-binding hot spots" on ACE2 and suggest that these mutations were naturally selected because they enhance viral interactions with either hACE2 or cACE2. These detailed mechanisms allow us to understand the events that led to the past SARS epidemic and to monitor the events that may lead to future SARS epidemics.

EXPERIMENTAL PROCEDURES

Protein Purification, Crystallization, and Structure Determination—SARS-CoV RBDs (from different viral strains) and ACE2 peptidase domains (human, civet, or chimeric) were expressed and purified as described previously (26, 27). In brief, the proteins containing an N-terminal honeybee melittin signal peptide and a C-terminal His tag were expressed in Sf9 insect cells using the Bac-to-Bac system (Invitrogen). The proteins were harvested from Sf9 cell supernatants and purified sequentially on a nickel-nitrilotriacetic acid column and a Superdex 200 gel filtration column (GE Healthcare). To purify the RBD-ACE2 complex, ACE2 was incubated with excess RBD, and then the complex was purified by gel filtration chromatography. RBD-ACE2 crystals were grown in sitting drops at room temperature over wells containing 100 mM Tris (pH 8.5), 20–24% PEG 6000, and 100 mM NaCl. Crystals were soaked briefly in 100 mM Tris (pH 8.5), 30% PEG 6000, 100 mM NaCl, and 30% ethylene glycol before being flash-frozen in liquid nitrogen. X-ray diffraction data were collected at Argonne Photon Source beamlines 19-ID and 24-ID and Advanced Light Source beamline 4.2.2. Each structure was determined by molecular replacement using the structure of hACE2 complexed with hTor02 RBD as the search model (Protein Data Bank code 2AJF). Data and refinement statistics are shown in Table 1. The software used for data processing and structure refinement is also listed in Table 1.

RBD/hACE2 Binding Assays—Surface plasmon resonance assays using a Biacore 2000 system were carried out as described previously (29, 30). In brief, to measure the binding affinities between mutant viral RBDs and wild-type ACE2, ACE2 was immobilized on a C5 sensor chip through direct covalent coupling via amine groups, and soluble RBDs were introduced at a flow rate of 20 μl/min at different concentrations (62.5, 125, and 250 nM). To measure the binding affinities between mutant ACE2 and wild-type viral RBDs, RBDs were immobilized on the sensor chip, and ACE2 was flowed through.

Pseudotyped Viral Infection Assays—Infection was assayed using murine leukemia viruses expressing β-galactosidase and pseudotyped with SARS-CoV spike protein as described previously (29). In brief, to prepare pseudotyped viruses, HEK293T cells were cotransfected with spike protein-encoding pcDNA3.1, p3240 expressing murine leukemia virus *gag* and *pol* genes, and a murine leukemia virus β-galactosidase-transducing vector (pBAG) (31). Viral supernatants were harvested and inoculated on HEK293T cells expressing ACE2 in pcDNA3.1. Infection efficiency was quantified by measuring β-galactosidase activity. The spike proteins and ACE2 contained a C-terminal C9 tag and HA tag, respectively. Hence, the concentrations of the spike protein packaged in pseudotyped viruses and of ACE2 expressed on the HEK293T cell surface were detected by Western blotting using anti-C9 and anti-HA antibodies, respectively, and quantified using ImageJ software (version 1.6) (supplemental Fig. S1). Compared with the infection experiments using fluorescence assays (32), the β-galactosidase assays used in this study are not as sensitive but are more stable and repeatable.

A

Strain	Host	Year	442	472	479	480	487
hTor02	human	2002-2003	Y	L	N	D	T
cSz02	civet	2002-2003	Y	L	K	D	S
hcGd03	human civet	2003-2004	Y	P	N	G	S
cHb05	civet	2005	Y	P	R	G	S
hHae08	human	2008	F	F	N	D	S
hOptimize	human	*In vitro* design	F	F	N	D	T
cOptimize	civet	*In vitro* design	Y	P	R	G	T

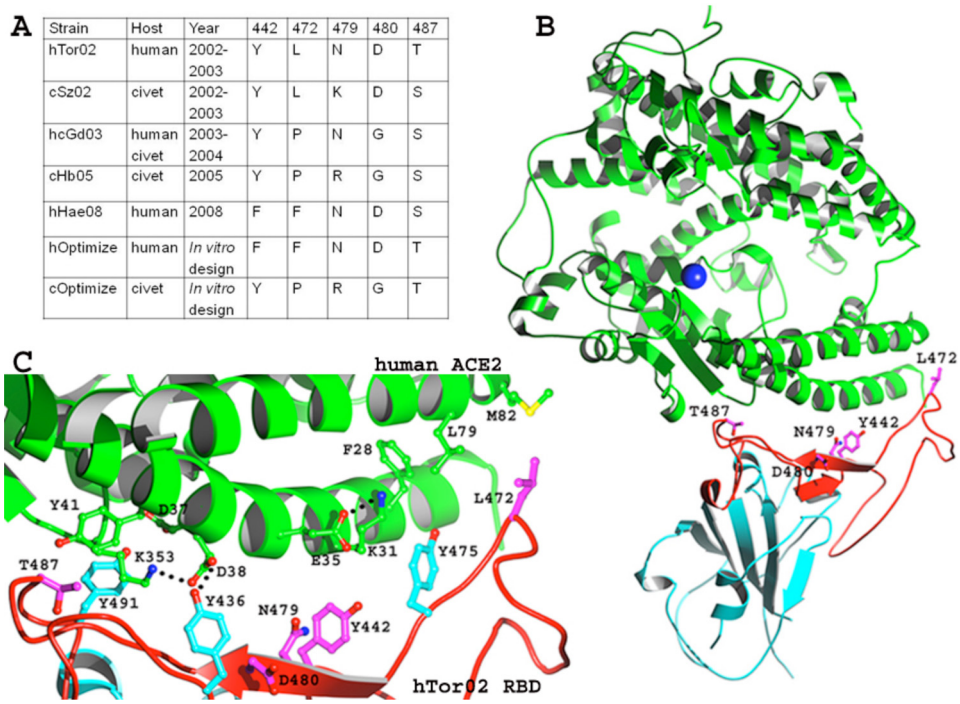

FIGURE 1. **Interface between SARS-CoV RBD and hACE2.** *A*, list of mutations in the RBMs of various SARS-CoV strains. Five representative existent strains and two predicted future strains are defined in the Introduction. *B*, overall structure of the hTor02 RBD-hACE2 complex (Protein Data Bank code 2AJF). hACE2 is in *green*, and hTor02 RBD is in *cyan* (core) and *red* (RBM). RBM residues that underwent mutations are displayed. *C*, detailed structure of the hTor02 RBD/hACE2 interface. hACE2 residues are in *green*, SARS-CoV residues that underwent mutations are in *magenta*, and SARS-CoV residues that played significant roles in the mutations are in *cyan*.

RESULTS AND DISCUSSIONS

Two Virus-binding Hot Spots on hACE2—All of the RBM mutations cluster around two virus-binding hot spots on hACE2, hot spot-31 and hot spot-353, which center on Lys-31 and Lys-353, respectively (Fig. 1*C*). Hot spot-353 is recognized by both SARS-CoV and human NL63 coronavirus, despite the markedly different structures of their RBDs (29, 30). Hot spot-31 is recognized by SARS-CoV only but not by NL63 coronavirus. The two hot spots have both structural similarities and dissimilarities. In unbound hACE2, both Lys-31 and Lys-353 point away from the protein and into solution (33). Upon SARS-CoV binding, both residues fold back, become buried in hydrophobic environments, and form salt bridges with hACE2 Glu-35 and Asp-38, respectively (26, 27). Because of the hydrophobic environments, formation of the salt bridges provides significant amounts of energy to the virus/receptor interactions. The difference between the two hot spots is that, upon salt bridge formation, Lys-353 is in a relatively extended conformation that is energetically favorable, whereas Lys-31 is in a strained conformation that is energetically unfavorable. In this study, we examined the structure and function of hot spot-31 by mutagenesis using surface plasmon resonance Biacore assays and pseudotyped viral infection assays (Fig. 2, *A* and *B*). Both assays showed that mutation K31A did not have a significant impact on RBD/hACE2 binding ($p > 0.10$ (t test) for both K_a and infection). In contrast, mutation K353A significantly decreased RBD/hACE2 binding affinity ($p < 0.01$ for both K_a and infection). These results suggest that there was a significant net energy gain from salt bridge formation at hot spot-353. In contrast, there was no significant net energy gain from salt bridge formation at hot spot-31, as the energy gain from salt bridge formation was cancelled out by loss from the strained conformation of Lys-31.

To further understand the structure and function of hot spot-31, we investigated mutation K31T in hACE2 based on the observation that cACE2, containing Thr-31, is an efficient receptor for hTor02 (Fig. 2*C*). Both Biacore and pseudotyped viral infection assays showed that mutation K31T significantly increased RBD/hACE2 binding affinity ($p < 0.001$ for both K_a and infection) (Fig. 2, *A* and *B*). To investigate the structural basis for mutation K31T, we determined the crystal structure of a human-civet chimeric ACE2 complexed with hTor02 RBD (Table 1). The chimeric ACE2 contained SARS-CoV-binding residues from cACE2 (Fig. 2*C*) and other residues from hACE2. We previously established this chimeric ACE2 as a useful alternative to cACE2 in crystallographic analysis of SARS-CoV/cACE2 interactions by showing that the chimeric ACE2 had the same receptor activities as cACE2 but the same crystallographic activities as hACE2 (27). The structure of the hTor02 RBD-chimeric ACE2 complex showed that a hydrogen bond between chimeric ACE2 Thr-31 and RBD Tyr-442 strengthens a hydrophobic network around hot spot-31 at the virus/receptor interface (Fig. 2*D*). Therefore, despite its insignificant net energy contribution, hot spot-31 plays an important role in RBD/ACE2 interactions. Consequently, upon introduction to a new species, SARS-CoV RBD may need to adapt to both hot spot-31 and hot spot-353 on ACE2.

Molecular Mechanisms of RBM Mutations in SARS-CoV—To investigate the molecular mechanisms of the RBM mutations, we introduced seven single mutations to hTor02 RBD,

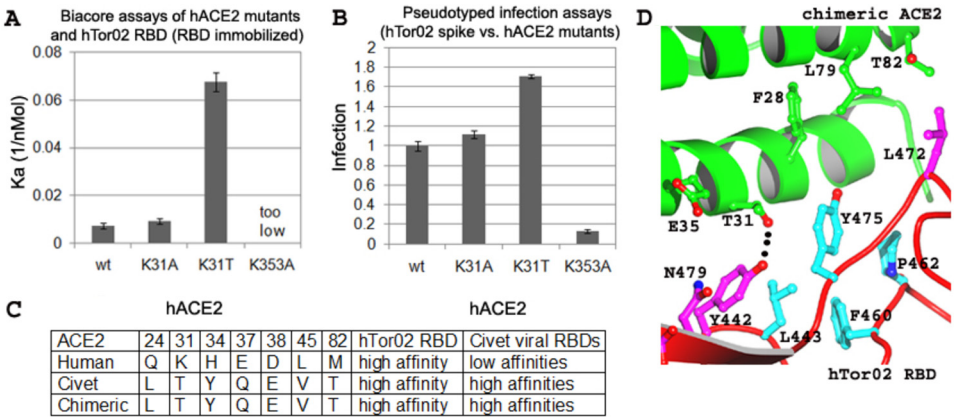

C

	hACE2							hACE2	
ACE2	24	31	34	37	38	45	82	hTor02 RBD	Civet viral RBDs
Human	Q	K	H	E	D	L	M	high affinity	low affinities
Civet	L	T	Y	Q	E	V	T	high affinity	high affinities
Chimeric	L	T	Y	Q	E	V	T	high affinity	high affinities

FIGURE 2. **Structures and functions of two virus-binding hot spots on hACE2.** *A*, surface plasmon resonance Biacore analysis of the binding interactions between hTor02 RBD and wild-type or mutant hACE2. hTor02 RBD was immobilized, and wild-type or mutant ACE2 was flowed through. Each experiment was repeated six times at three different protein concentrations. The corresponding S.E. values are shown. *B*, pseudotyped viral infection assays of the interactions between hTor02 spike protein and wild-type or mutant hACE2. Retroviral murine leukemia viruses expressing β-galactosidase and pseudotyped with hTor02 spike protein were used to infect HEK293T cells expressing wild-type or mutant hACE2. Infection efficiency of pseudotyped viruses was measured by β-galactosidase assays and normalized against the infection efficiency in cells expressing wild-type hACE2. Each experiment was repeated six times. The corresponding S.E. values are shown. *C*, use of a human-civet chimeric ACE2 in crystallographic studies of RBD/cACE2 interactions. The chimeric ACE2 contains SARS-CoV-binding residues from cACE2 and other residues from hACE2. The chimeric ACE2 has the same receptor activities as cACE2 but the same crystallographic activities as hACE2 (27). SARS-CoV-binding residues that differ between hACE2 and cACE2 are shown. *D*, structure of the interface between hTor02 RBD and the chimeric ACE2.

TABLE 1

Crystallographic data collection and refinement statistics

X-ray diffraction data were processed using HKL2000 (35). Programs CNS (36) and CCP4 REFMAC (37) were used for structure refinement. Structural illustrations were made using POVscript (38). r.m.s.d., root mean square deviation.

	Complex			
	hTor02 RBD-chimeric ACE2	**hOptimize RBD-hACE2**	**cOptimize RBD-chimeric ACE2**	**cOptimize RBD-hACE2**
Data				
Space group	$P2_1$	$P2_1$	$P2_1$	$P2_1$
Cell constants	a = 81.6, b = 119.5, c = 113.4 Å; β = 92.5°	a = 81.4, b = 118.3, c = 111.9 Å; β = 93.15°	a = 81.0, b = 120.0, c = 112.2 Å; β = 93.15°	a = 81.2, b = 119.3, c = 113.2 Å; β = 92.25°
Resolution (Å)	50–3.0	50–2.9	50–3.0	50–3.0
R_{sym} (last shell) (%)	9.8 (61.6)	7.5 (33.4)	7.0 (51.6)	9.2 (48.0)
Observed reflections	157,444	223,385	122,747	296,564
Unique reflections	42,738	47,509	42,870	44,284
Completeness (last shell) (%)	97.7 (95.1)	93.4 (59.1)	91.7 (59.9)	95.1 (67.0)
I/σ (last shell)	6.3 (1.2)	11.4 (3.2)	16.5 (1.6)	20.2 (2.2)
Refinement				
R_{work} (R_{free}) (%)	23.9 (29.2)	22.6 (28.3)	23.9 (28.5)	23.0 (27.8)
R_{free} reflections (%)	5	5	5	5
Bond length r.m.s.d. (Å)	0.012	0.010	0.011	0.010
Bond angle r.m.s.d.	1.361°	1.252°	1.329°	1.257°
Chiral r.m.s.d. (Å^3)	0.092	0.090	0.086	0.083

Y442F, L472P, L472F, N479K, N479R, D480G, and T487S, corresponding to all of the RBM mutations identified in human and civet SARS-CoV strains (Fig. 1*A*). We expressed and purified each of these mutant RBDs and measured their binding affinities for hACE2 and cACE2 using Biacore assays (Fig. 3, *A* and *B*). The results showed that hTor02 RBD bound to hACE2 and cACE2 with similar K_a values ($p > 0.50$). The affinity of hTor02 RBD for hACE2 was increased by Y442F and L472F ($p < 0.01$); unchanged by N479R ($p > 0.10$); and decreased by L472P, D480G, N479K, and T487S ($p < 0.02$) (Fig. 3*A*). The affinity of hTor02 RBD for cACE2 was increased by N479R and D480G ($p < 0.01$); unchanged by L472P and N479K ($p > 0.50$); and decreased by L472F, Y442F, and T487S ($p < 0.01$) (Fig. 3*B*). In sum, among the RBM residues that have been identified in different SARS-CoV strains, Phe-442, Phe-472, Asn-479/Arg-479, Asp-480, and Thr-487 enhanced RBD/hACE2 interactions, whereas Tyr-442, Pro-472/Leu-472, Arg-479, Gly-480 and Thr-487 enhanced RBD/cACE2 interactions.

The above results suggest that combinations of the RBM residues that enhance RBD/hACE2 or RBD/cACE2 interactions can potentially produce new RBDs with exceptionally high affinity for hACE2 or cACE2, respectively. To test this hypothesis, we designed and constructed two such new RBDs: hOptimize RBD containing Phe-442, Phe-472, Asn-479, Asp-480, and Thr-487 and cOptimize RBD containing Tyr-442, Pro-472, Arg-479, Gly-480, and Thr-487 (Fig. 1*A*). We expressed and purified each of the RBDs. Biacore assays confirmed that compared with hTor02 RBD, hOptimize and cOptimize RBDs had higher affinities for hACE2 and cACE2, respectively ($p < 0.01$) (Fig. 3, *A* and *B*). On the other hand, whereas hOptimize RBD had low affinity for cACE2, cOptimize RBD had substantial affinity for hACE2.

Structural Mechanisms of RBM Mutations in SARS-CoV—To investigate the structural mechanisms of the RBM mutations, we determined the following three crystal structures: hOptimize RBD complexed with hACE2, cOptimize RBD complexed with the chimeric ACE2, and hOptimize RBD complexed

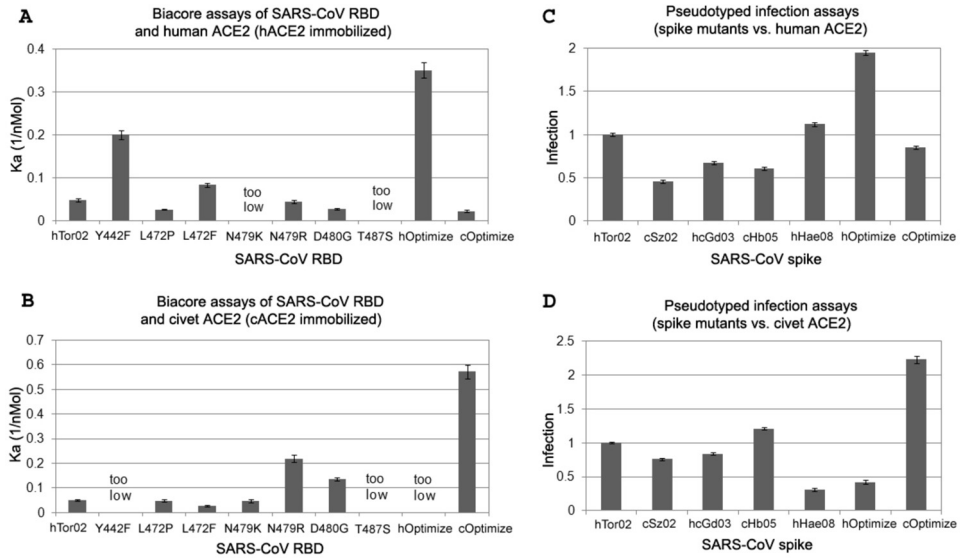

FIGURE 3. **Molecular mechanisms of RBM mutations in SARS-CoV.** *A*, surface plasmon resonance Biacore analysis of the binding interactions between hACE2 and wild-type or mutant hTor02 RBD. hACE2 was immobilized, and wild-type or mutant hTor02 RBD was flowed through. *B*, surface plasmon resonance Biacore analysis of the binding interactions between cACE2 and wild-type or mutant hTor02 RBD. cACE2 was immobilized, and wild-type or mutant hTor02 RBD was flowed through. *C*, pseudotyped viral infection assays of the interactions between different spike proteins and hACE2. *D*, pseudotyped viral infection assays of the interactions between different spike proteins and cACE2.

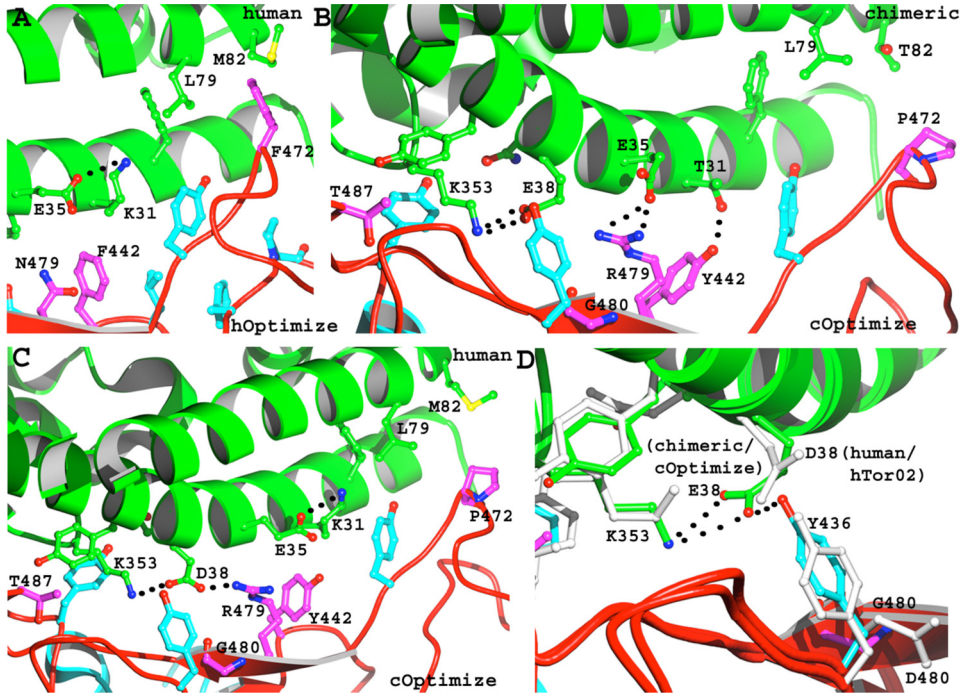

FIGURE 4. **Structural mechanisms of RBM mutations in SARS-CoV.** *A*, structure of the interface between hACE2 and hOptimize RBD. *B*, structure of the interface between the chimeric ACE2 and cOptimize RBD. *C*, structure of the interface between hACE2 and cOptimize RBD. *D*, superimposed structures of the interfaces between the chimeric ACE2 and cOptimize RBD (*colored*) and between hACE2 and hTor02 (*white*).

with the chimeric ACE2 (Fig. 4 and Table 1). Together, these structures show that naturally selected RBM mutations either strengthened favorable interactions or reduced unfavorable interactions with the two virus-binding hot spots on ACE2. The structural details of each of the RBM mutations are as follow.

RBD residue 442 interacts with hot spot-31 on ACE2. At the RBD/hACE2 interfaces, the hydroxyl group of Tyr-442 has partial steric clash with the alkyl side chain of hACE2 Lys-31 (Fig. 1*C*). Mutation Y442F removes this hydroxyl group, partially releases the structural strain of Lys-31 (Fig. 4*A*), and increases the RBD/hACE2 binding affinity. As discussed above, at the RBD/chimeric ACE2 interfaces, the hydroxyl group of Tyr-442 forms a critical hydrogen bond with chimeric ACE2 Thr-31 (Figs. 2*D* and 4*B*). Mutation Y442F removes this hydrogen bond, weakens the hydrophobic network around hot spot-31, and decreases the RBD/cACE2 binding affinity. Therefore, Phe-442 and Tyr-442 were viral adaptations to hACE2 and cACE2, respectively (Fig. 5).

Residues in SARS-CoV RBD	SARS-CoV adaptation to human ACE2	SARS-CoV adaptation to civet ACE2
442	Y → F	F → Y
472	P → L → F	F → L ⇄ P
479	K → N K → R	N ⇄ K → R
480	G → D	D → G
487	S → T	S → T

FIGURE 5. **Summary of host receptor adaptation by SARS-CoV.** Listed are adaptations of RBM residues to hACE2 or cACE2. *Arrows* point from less well adapted residues to better adapted residues. *Double arrows* connect equally well adapted residues.

RBD residue 472 interacts with hot spot-31 on ACE2. At the RBD/hACE2 interfaces, Leu-472 forms favorable hydrophobic interactions with hACE2 Met-82 and Leu-79 and strengthens the hydrophobic network around hot spot-31 (Fig. 1*C*). Mutation L472F further strengthens but mutation L472P weakens RBD/hACE2 interactions (Fig. 4, *A* and *C*). At the RBD/chimeric ACE2 interfaces, Phe-472 would have partial steric clash with the hydroxyl group of chimeric ACE2 Thr-82 (Figs. 2*D* and 4*B*), and hence, mutation L472F decreases the RBD/cACE2 binding affinity. Additionally, neither Leu-472 nor Pro-472 has significant contact with Thr-82 (Figs. 2*D* and 4*B*), and hence, mutation L472P has no significant effects on the RBD/cACE2 interactions. Therefore, Phe-472 and Pro-472/Leu-472 were viral adaptations to hACE2 and cACE2, respectively (Fig. 5).

RBD residue 479 interacts with both hot spots on ACE2. As shown previously, at the RBD/hACE2 interfaces, mutation N479K introduces a positive charge that can compete with hACE2 Lys-31 for hACE2 Glu-35 as a salt bridge partner (26, 27), and hence, it decreases the RBD/hACE2 binding affinity. Unexpectedly, unlike N479K, mutation N479R has no significant effects on the RBD/hACE2 binding affinity even though it does introduce a positive charge. This is because Arg-479 and hACE2 Lys-353 can both form a salt bridge with hACE2 Asp-38 (Fig. 4*C*). At the RBD/chimeric ACE2 interfaces, Thr-31 cannot form a salt bridge with chimeric ACE2 Glu-35 (Figs. 2*D* and 4*B*), and hence, Glu-35 is available to form a salt bridge with Lys-479. On the other hand, Lys-479 has high conformational entropy and stacks poorly with the hydrophobic network around hot spot-31 (27). Consequently, mutation N479K has no significant effects on the RBD/cACE2 binding affinity. In contrast, Arg-479 can form a strong bifurcated salt bridge with Glu-35 and is also a much better hydrophobic stacker than Lys-479 (Fig. 4*B*). Thus, mutation N479R increases the RBD/cACE2 binding affinity. Therefore, Asn-479/Arg-479 and Arg-479 were viral adaptations to hACE2 and cACE2, respectively (Fig. 5).

RBD residue 480 interacts with hot spot-353 on ACE2. At the RBD/hACE2 interfaces, RBD Tyr-436 forms a hydrogen bond with hACE2 Asp-38 and strengthens the Lys-353–Asp-38 salt bridge (Figs. 1*C* and 4*D*). The alkyl side chain of Asp-480 forms a hydrophobic interaction with Tyr-436 and supports the Tyr-436–Asp-38 hydrogen bond. Consequently, mutation D480G weakens the above interactions and decreases the RBD/hACE2 binding affinity. At the RBD/chimeric ACE2 interfaces, chimeric ACE2 Glu-38, which has a longer side chain than hACE2 Asp-38, moves back to keep the salt bridge with Lys-353. Accordingly, Tyr-436 also needs to move to keep the hydrogen bond with Glu-38 (Fig. 4*D*). Mutation D480G facilitates the movement of Tyr-436 and increases the RBD/cACE2 binding affinity. Therefore, Asp-480 and Gly-480 were viral adaptations to hACE2 and cACE2, respectively (Fig. 5).

RBD residue 487 interacts with hot spot-353 on hACE2. As shown previously, at the RBD/hACE2 interfaces, the methyl group of Thr-487 supports the Lys-353–Asp-38 salt bridge (Fig. 1*C*) (26, 27), and hence, mutation T487S decreases the RBD/hACE2 binding affinity. At the RBD/chimeric ACE2 interfaces, the methyl group of Thr-487 also supports the Lys-353–Glu-38 salt bridge (Fig. 4*B*), and thus, mutation T487S decreases the RBD/cACE2 binding affinity. Therefore, Thr-487 was a viral adaptation to both hACE2 and cACE2 (Fig. 5).

Evaluation of Host Cell Infections Mediated by Different SARS-CoV Spike Proteins—To further investigate the interactions between different RBDs and ACE2 from humans or civets, we measured the spike protein-mediated infection of hACE2- or cACE2-expressing cells using pseudotyped viral infection assays (Fig. 3, *C* and *D*). Compared with Biacore assays that directly measure binding interactions between monomeric RBD and monomeric ACE2 in solution, pseudotyped infection assays measure binding interactions between trimeric spike proteins on viral surfaces and monomeric ACE2 on target cell surfaces. In addition, pseudotyped infection assays require not only receptor binding but also membrane fusion and post-fusion steps for reporter gene expression. Hence, pseudotyped infection assays reflect more truthfully than Biacore assays on how the RBM mutations may impact SARS-CoV infectivity and pathogenesis.

The spike proteins used in the assays share the same sequences as the hTor02 spike protein except that their RBDs contain different combinations of RBM residues (Fig. 1*A*). hOptimize spike protein mediated a higher level of infection of hACE2-expressing cells than all other spike proteins ($p < 0.01$) because its residues at positions 442, 472, 479, 480, and 487 were all best adapted to hACE2 (Fig. 3*C*). Particularly, hOptimize spike protein-pseudotyped viruses infected hACE2-expressing cells about twice as efficiently as hTor02 spike protein-pseudotyped viruses and ~4-fold as efficiently as cSz02 spike protein-pseudotyped viruses. Additionally, hOptimize spike protein mediated a lower level of infection of cACE2-expressing cells than all other spike proteins except hHae08 ($p < 0.01$) because its residues at four of the above positions, except position 487, were poorly adapted to cACE2. On the other hand, cOptimize spike protein mediated a higher level of infection of cACE2-expressing cells than all other spike proteins ($p < 0.01$) because its residues at the above five positions were all best adapted to cACE2 (Fig. 3*D*). Particularly, cOptimize spike protein-pseudotyped viruses infected cACE2-expressing cells about twice as efficiently as hTor02 spike protein-pseudotyped viruses and ~7-fold as efficiently as hHae08 spike protein-pseudotyped viruses. cOptimize spike protein also mediated a substantial level of infection of hACE2-expressing cells, lower than hTor02 but significantly higher than hcGd03 ($p < 0.01$), because its residues at positions 479 and 487 were well

adapted to hACE2, whereas its residues at the other three positions were poorly adapted to hACE2. Overall, the results from the pseudotyped infection assays correlate well with those from Biacore data and structural analysis.

Monitoring Future SARS-CoV Evolution in Animals—SARS-CoV evolution in animals needs to be carefully monitored as a preventive measure for potential future SARS epidemics. SARS-CoV was found in wild civets in 2005 (9) and can potentially cross the species barrier to infect humans again, as it did as least twice before. Novel coronaviruses have been identified in bats (13, 14), and some of these bat coronaviruses may be transmitted to humans either directly or through some intermediate animal hosts (11). SARS-CoV may also be misused as a bioweapon to infect humans. Regardless of the circumstances under which SARS-CoV re-emerges, understanding the mechanisms of its host receptor adaptation will be crucial for dealing with its re-emergence.

In this study, we have identified RBM residues that are best adapted to hACE2 or cACE2, and hence, these residues can be predictors of future SARS-CoV evolution in animals. The elucidated receptor recognition mechanisms by SARS-CoV can allow us to evaluate the potential epidemical consequences of a future SARS-CoV strain simply by examining its genomic sequence. For example, if a future SARS-CoV strain is isolated from civets or humans, we will be able to evaluate the binding affinity between its RBD and cACE2 or hACE2 based on its RBM sequences. More specifically, if a future SARS-CoV strain contains a majority or all of the cACE2-adapted RBM residues, it can potentially have high infectivity for civet cells; if it contains a majority or all of the hACE2-adapted RBM residues, it can potentially have high infectivity for human cells. Moreover, the detailed interactions between SARS-CoV RBD and the two virus-binding hot spots on ACE2 as elucidated in this study will help us understand and evaluate new RBM mutations in future SARS-CoV strains that are different from the previously identified RBM mutations. The results from this study can also contribute to the monitoring and control of SLCVs in bats by providing insights into how these bat viruses may interact with the ACE2 molecules from bats, civets, humans, or other animals (27, 34). It should be noted that our study did not include replication-competent viruses or animal models, and thus, future studies will be required to establish the correlation between optimized RBDs and infectivities of live SARS-CoV strains. To conclude, given that SARS-CoV may still be evolving in civets and that SLCVs are harbored by bats, it remains possible for SARS-CoV to re-emerge into the human population through civets or other animals, but we can be better prepared to prevent or handle future outbreaks of the virus with improved understanding of the mechanisms for its host receptor adaptation.

Acknowledgments—We thank Drs. Kathryn Holmes, Ralph Baric, Carrie Wilmot, and Yuhong Jiang for discussion and comments and the staff at Argonne Photon Source beamlines 19-ID and 24-ID and at Advanced Light Source beamline 4.2.2 for assistance in data collection. Computer resources were provided by the Basic Sciences Computing Laboratory of the University of Minnesota Supercomputing Institute.

REFERENCES

1. Lee, N., Hui, D., Wu, A., Chan, P., Cameron, P., Joynt, G. M., Ahuja, A., Yung, M. Y., Leung, C. B., To, K. F., Lui, S. F., Szeto, C. C., Chung, S., and Sung, J. J. (2003) A major outbreak of severe acute respiratory syndrome in Hong Kong. *N. Engl. J. Med.* **348,** 1986–1994
2. Yu, I. T., Li, Y.., Wong, T. W., Tam, W., Chan, A. T., Lee, J. H., Leung, D. Y., and Ho, T. (2004) Evidence of airborne transmission of the severe acute respiratory syndrome virus. *N. Engl. J. Med.* **350,** 1731–1739
3. Marra, M. A., Jones, S. J., Astell, C. R., Holt, R. A., Brooks-Wilson, A., Butterfield, Y. S., Khattra, J., Asano, J. K., Barber, S. A., Chan, S. Y., Cloutier, A., Coughlin, S. M., Freeman, D., Girn, N., Griffith, O. L., Leach, S. R., Mayo, M., McDonald, H., Montgomery, S. B., Pandoh, P. K., Petrescu, A. S., Robertson, A. G., Schein, J. E., Siddiqui, A., Smailus, D. E., Stott, J. M., Yang, G. S., Plummer, F., Andonov, A., Artsob, H., Bastien, N., Bernard, K., Booth, T. F., Bowness, D., Czub, M., Drebot, M., Fernando, L., Flick, R., Garbutt, M., Gray, M., Grolla, A., Jones, S., Feldmann, H., Meyers, A., Kabani, A., Li, Y., Normand, S., Stroher, U., Tipples, G. A., Tyler, S., Vogrig, R., Ward, D., Watson, B., Brunham, R. C., Krajden, M., Petric, M., Skowronski, D. M., Upton, C., and Roper, R. L. (2003) The genome sequence of the SARS-associated coronavirus. *Science* **300,** 1399–1404
4. Peiris, J. S., Lai, S. T., Poon, L. L., Guan, Y., Yam, L. Y., Lim, W., Nicholls, J., Yee, W. K., Yan, W. W., Cheung, M. T., Cheng, V. C., Chan, K. H., Tsang, D. N., Yung, R. W., Ng, T. K., and Yuen, K. Y. (2003) Coronavirus as a possible cause of severe acute respiratory syndrome. *Lancet* **361,** 1319–1325
5. Guan, Y., Zheng, B. J., He, Y. Q., Liu, X. L., Zhuang, Z. X., Cheung, C. L., Luo, S. W., Li, P. H., Zhang, L. J., Guan, Y. J., Butt, K. M., Wong, K. L., Chan, K. W., Lim, W., Shortridge, K. F., Yuen, K. Y., Peiris, J. S., and Poon, L. L. (2003) Isolation and characterization of viruses related to the SARS coronavirus from animals in southern China. *Science* **302,** 276–278
6. Liang, G., Chen, Q., Xu, J., Liu, Y., Lim, W., Peiris, J. S., Anderson, L. J., Ruan, L., Li, H., Kan, B., Di, B., Cheng, P., Chan, K. H., Erdman, D. D., Gu, S., Yan, X., Liang, W., Zhou, D., Haynes, L., Duan, S., Zhang, X., Zheng, H., Gao, Y., Tong, S., Li, D., Fang, L., Qin, P., Xu, W., and SARS Diagnosis Working Group (2004) Laboratory diagnosis of four recent sporadic cases of community-acquired SARS, Guangdong Province, China. *Emerging Infectious Diseases* **10,** 1774–1781
7. Song, H. D., Tu, C. C., Zhang, G. W., Wang, S. Y., Zheng, K., Lei, L. C., Chen, Q. X., Gao, Y. W., Zhou, H. Q., Xiang, H., Zheng, H. J., Chern, S. W., Cheng, F., Pan, C. M., Xuan, H., Chen, S. J., Luo, H. M., Zhou, D. H., Liu, Y. F., He, J. F., Qin, P. Z., Li, L. H., Ren, Y. Q., Liang, W. J., Yu, Y. D., Anderson, L., Wang, M., Xu, R. H., Wu, X. W., Zheng, H. Y., Chen, J. D., Liang, G., Gao, Y., Liao, M., Fang, L., Jiang, L. Y., Li, H., Chen, F., Di, B., He, L. J., Lin, J. Y., Tong, S., Kong, X., Du, L., Hao, P., Tang, H., Bernini, A., Yu, X. J., Spiga, O., Guo, Z. M., Pan, H. Y., He, W. Z., Manuguerra, J. C., Fontanet, A., Danchin, A., Niccolai, N., Li, Y. X., Wu, C. I., and Zhao, G. P. (2005) Cross-host evolution of severe acute respiratory syndrome coronavirus in palm civet and human. *Proc. Natl. Acad. Sci. U.S.A.* **102,** 2430–2435
8. Chinese SARS Molecular Epidemiology Consortium (2004) Molecular evolution of the SARS coronavirus during the course of the SARS epidemic in China. *Science* **303,** 1666–1669
9. Liu, L., Fang, Q., Deng, F., Wang, H., Yi, C. E., Ba, L., Yu, W., Lin, R. D., Li, T., Hu, Z., Ho, D. D., Zhang, L., and Chen, Z. (2007) Natural mutations in the receptor-binding domain of spike glycoprotein determine the reactivity of cross-neutralization between palm civet coronavirus and severe acute respiratory syndrome coronavirus. *J. Virol.* **81,** 4694–4700
10. Sheahan, T., Rockx, B., Donaldson, E., Sims, A., Pickles, R., Corti, D., and Baric, R. (2008) Mechanisms of zoonotic severe acute respiratory syndrome coronavirus host range expansion in human airway epithelium. *J. Virol.* **82,** 2274–2285
11. Li, W., Wong, S. K., Li, F., Kuhn, J. H., Huang, I. C., Choe, H., and Farzan, M. (2006) Animal origins of the severe acute respiratory syndrome coronavirus: insight from ACE2-S-protein interactions. *J. Virol.* **80,** 4211–4219
12. Kan, B., Wang, M., Jing, H., Xu, H., Jiang, X., Yan, M., Liang, W., Zheng, H., Wan, K., Liu, Q., Cui, B., Xu, Y., Zhang, E., Wang, H., Ye, J., Li, G., Li, M.,

Cui, Z., Qi, X., Chen, K., Du, L., Gao, K., Zhao, Y. T., Zou, X. Z., Feng, Y. J., Gao, Y. F., Hai, R., Yu, D., Guan, Y., and Xu, J. (2005) Molecular evolution analysis and geographic investigation of severe acute respiratory syndrome coronavirus-like virus in palm civets at an animal market and on farms. *J. Virol.* **79,** 11892–11900

13. Lau, S. K., Woo, P. C., Li, K. S., Huang, Y., Tsoi, H. W., Wong, B. H., Wong, S. S., Leung, S. Y., Chan, K. H., and Yuen, K. Y. (2005) Severe acute respiratory syndrome coronavirus-like virus in Chinese horseshoe bats. *Proc. Natl. Acad. Sci. U.S.A.* **102,** 14040–14045
14. Li, W., Shi, Z., Yu, M., Ren, W., Smith, C., Epstein, J. H., Wang, H., Crameri, G., Hu, Z., Zhang, H., Zhang, J., McEachern, J., Field, H., Daszak, P., Eaton, B. T., Zhang, S., and Wang, L. F. (2005) Bats are natural reservoirs of SARS-like coronaviruses. *Science* **310,** 676–679
15. Ren, W., Qu, X., Li, W., Han, Z., Yu, M., Zhou, P., Zhang, S. Y., Wang, L. F., Deng, H., and Shi, Z. (2008) Difference in receptor usage between severe acute respiratory syndrome (SARS) coronavirus and SARS-like coronavirus of bat origin. *J. Virol.* **82,** 1899–1907
16. Li, W., Moore, M. J., Vasilieva, N., Sui, J., Wong, S. K., Berne, M. A., Somasundaran, M., Sullivan, J. L., Luzuriaga, K., Greenough, T. C., Choe, H., and Farzan, M. (2003) Angiotensin-converting enzyme 2 is a functional receptor for the SARS coronavirus. *Nature* **426,** 450–454
17. Li, F., Berardi, M., Li, W., Farzan, M., Dormitzer, P. R., and Harrison, S. C. (2006) Conformational states of the severe acute respiratory syndrome coronavirus spike protein ectodomain. *J. Virol.* **80,** 6794–6800
18. Lai, M. M., and Holmes, K. V. (2001) in *Fields Virology* (Knipe, D. M., and Howley, P. M., eds) pp. 1163–1186, Lippincott Williams & Wilkins, Philadelphia, PA
19. Xu, Y., Lou, Z., Liu, Y., Pang, H., Tien, P., Gao, G. F., and Rao, Z. (2004) Crystal structure of severe acute respiratory syndrome coronavirus spike protein fusion core. *J. Biol. Chem.* **279,** 49414–49419
20. Babcock, G. J., Esshaki, D. J., Thomas, W. D., Jr., and Ambrosino, D. M. (2004) Amino acids 270–510 of the severe acute respiratory syndrome coronavirus spike protein are required for interaction with receptor. *J. Virol.* **78,** 4552–4560
21. Wong, S. K., Li, W., Moore, M. J., Choe, H., and Farzan, M. (2004) A 193-amino acid fragment of the SARS coronavirus S protein efficiently binds angiotensin-converting enzyme 2. *J. Biol. Chem.* **279,** 3197–3201
22. Xiao, X., Chakraborti, S., Dimitrov, A. S., Gramatikoff, K., and Dimitrov, D. S. (2003) The SARS-CoV S glycoprotein: expression and functional characterization. *Biochem. Biophys. Res. Commun.* **312,** 1159–1164
23. Li, W., Greenough, T. C., Moore, M. J., Vasilieva, N., Somasundaran, M., Sullivan, J. L., Farzan, M., and Choe, H. (2004) Efficient replication of severe acute respiratory syndrome coronavirus in mouse cells is limited by murine angiotensin-converting enzyme 2. *J. Virol.* **78,** 11429–11433
24. Li, W., Zhang, C., Sui, J., Kuhn, J. H., Moore, M. J., Luo, S., Wong, S. K., Huang, I. C., Xu, K., Vasilieva, N., Murakami, A., He, Y., Marasco, W. A., Guan, Y., Choe, H., and Farzan, M. (2005) Receptor and viral determinants of SARS-coronavirus adaptation to human ACE2. *EMBO J.* **24,** 1634–1643
25. McCray, P. B., Jr., Pewe, L., Wohlford-Lenane, C., Hickey, M., Manzel, L., Shi, L., Netland, J., Jia, H. P., Halabi, C., Sigmund, C. D., Meyerholz, D. K., Kirby, P., Look, D. C., and Perlman, S. (2007) Lethal infection of K18-*hACE2* mice infected with severe acute respiratory syndrome coronavirus. *J. Virol.* **81,** 813–821
26. Li, F., Li, W., Farzan, M., and Harrison, S. C. (2005) Structure of SARS coronavirus spike receptor-binding domain complexed with receptor. *Science* **309,** 1864–1868
27. Li, F. (2008) Structural analysis of major species barriers between humans and palm civets for severe acute respiratory syndrome coronavirus infections. *J. Virol.* **82,** 6984–6991
28. Qu, X. X., Hao, P., Song, X. J., Jiang, S. M., Liu, Y. X., Wang, P. G., Rao, X., Song, H. D., Wang, S. Y., Zuo, Y., Zheng, A. H., Luo, M., Wang, H. L., Deng, F., Wang, H. Z., Hu, Z. H., Ding, M. X., Zhao, G. P., and Deng, H. K. (2005) Identification of two critical amino acid residues of the severe acute respiratory syndrome coronavirus spike protein for its variation in zoonotic tropism transition via a double substitution strategy. *J. Biol. Chem.* **280,** 29588–29595
29. Wu, K., Chen, L., Peng, G., Zhou, W., Pennell, C. A., Mansky, L. M., Geraghty, R. J., and Li, F. (2011) A virus-binding hot spot on human angiotensin-converting enzyme 2 is critical for binding of two different coronaviruses. *J. Virol.* **85,** 5331–5337
30. Wu, K., Li, W., Peng, G., and Li, F. (2009) Crystal structure of NL63 respiratory coronavirus receptor-binding domain complexed with its human receptor. *Proc. Natl. Acad. Sci. U.S.A.* **106,** 19970–19974
31. Price, J., Turner, D., and Cepko, C. (1987) Lineage analysis in the vertebrate nervous system by retrovirus-mediated gene transfer. *Proc. Natl. Acad. Sci. U.S.A.* **84,** 156–160
32. Peng, G., Sun, D., Rajashankar, K. R., Qian, Z., Holmes, K. V., and Li, F. (2011) Crystal structure of mouse coronavirus receptor-binding domain complexed with its murine receptor. *Proc. Natl. Acad. Sci. U.S.A.* **108,** 10696–10701
33. Towler, P., Staker, B., Prasad, S. G., Menon, S., Tang, J., Parsons, T., Ryan, D., Fisher, M., Williams, D., Dales, N. A., Patane, M. A., and Pantoliano, M. W. (2004) ACE2 X-ray structures reveal a large hinge-bending motion important for inhibitor binding and catalysis. *J. Biol. Chem.* **279,** 17996–18007
34. Hou, Y., Peng, C., Yu, M., Li, Y., Han, Z., Li, F., Wang, L. F., and Shi, Z. (2010) Angiotensin-converting enzyme 2 (ACE2) proteins of different bat species confer variable susceptibility to SARS-CoV entry. *Arch. Virol.* **155,** 1563–1569
35. Otwinowski, Z., and Minor, W. (1997) Processing of x-ray diffraction data collected in oscillation mode. *Methods Enzymol.* **276,** 307–326
36. Brünger, A. T., Adams, P. D., Clore, G. M., DeLano, W. L., Gros, P., Grosse-Kunstleve, R. W., Jiang, J. S., Kuszewski, J., Nilges, M., Pannu, N. S., Read, R. J., Rice, L. M., Simonson, T., and Warren, G. L. (1998) Crystallography & NMR system: A new software suite for macromolecular structure determination. *Acta Crystallogr. D Biol. Crystallogr.* **54,** 905–921
37. Murshudov, G. N., Vagin, A. A., Lebedev, A., Wilson, K. S., and Dodson, E. J. (1999) Efficient anisotropic refinement of macromolecular structures using FFT. *Acta Crystallogr. D Biol. Crystallogr.* **55,** 247–255
38. Fenn, T. D., Ringe, D., and Petsko, G. A. (2003) *POVScript+*: a program for model and data visualization using persistence of vision ray-tracing. *J. Appl. Crystallogr.* **36,** 944–947